Analysis of particle induced dislocation structures using three-dimensional dislocation dynamics and strain gradient plasticity

Hyung-Jun Chang [a,*], Anaïs Gaubert [b], Marc Fivel [c], Stéphane Berbenni [d], Olivier Bouaziz [a,e], Samuel Forest [a,*]

[a] Centre des Matériaux, Mines ParisTech, CNRS UMR7633 BP87, 91003 Evry, France
[b] ONERA, BP72, 92322 Chatillon Cedex, France
[c] SIMaP-GPM2, Grenoble INP/CNRS UMR 5266, BP46, Domaine Universitaire, 38402 St. Martin d'Hères Cedex, France
[d] LPMM, CNRS, Arts et Métiers Metz, Technopole 57078, Metz Cedex 03, France
[e] ArcelorMittal Research, Voie Romaine-BP30320, 57283 Maizieres-les-Metz Cedex, France

ARTICLE INFO

ABSTRACT

Investigations of precipitation hardening are performed in term of analysis of distributions of geometrically necessary dislocations (GND) surrounding particles. The dislocation microstructures are computed from three dimensional discrete dislocation dynamics (DDD) and strain gradient plasticity (SGP) models. DDD simulations of spherical particle embedded in a single crystal matrix undergoing single slip provide the GND structures and the associated work-hardening. A 3D periodic arrangement of particles with cubic symmetry is considered. It is found that a network of slip and kink deformation bands develops, which is strongly dependent on the crystal lattice orientation of the matrix with respect to the particle array. For some relative orientations, the strain hardening is increased by the distributions of GND which act as additional barrier against slip. Some of these features are also captured with the SGP model in contrast to conventional continuum crystal plasticity.

© 2011 Elsevier B.V. All rights reserved.

1. Introduction

In crystal plasticity, precipitation hardening is commonly associated to a yield strength increase. The hardening can be explained by the formation of typical dislocation structures around particles, made of geometrically necessary dislocations (GND). Such dislocation microstructures have also been evidenced experimentally [1,2]. The aim of this work is to describe the relationship between the GND structure and the matrix crystal lattice orientation using computational analysis.

During the last few years, many numerical models have been developed with the aim to investigate GND structures around particles [3]. Some of them are based on generalized continuum mechanics. As an example, the strain gradient plasticity (SGP) models are based on the dislocation density tensor directly related to GND densities [4]. Some relationships have then been established between the SGP constitutive equations and specific dislocation structures like pile-up formation at interfaces [5]. Most of these studies are however restricted to two-dimensional computations so that no relationship have been derived yet within a full 3D framework.

Other models, such as discrete dislocation dynamics (DDD) are explicitly dealing with dislocation lines. Obviously, DDD give access to the dislocation microstructure and consequently the evolution of the GND quantities as a result of collective interactions. 2D and 3D DDD simulations are expected to provide a physics-based description of crystal plasticity. Therefore, it is widely believed that DDD simulations can bridge the gap from the physical origin of plasticity to continuum models. This technique has already been applied in 3D to the question of precipitation hardening but without any detailed description of the dislocation structures around particles [6].

In this paper, GND distributions are investigated in 3D using DDD [7] and SGP [8] simulations of periodic sets of spherical particles embedded in a single crystal matrix loaded in pure shear. Only single slip is considered as a first step for the understanding of 3D particle hardening. DDD simulations show that the dislocation microstructure develops as wall-like structures which strongly depends on the slip system orientation with respect to the array of particles. The physical meaning and origin of the dislocation spreading are analyzed and discussed. They are interpreted as a network of slip and kink bands. A simple three-dimensional SGP model based on the micromorphic approach is then used to predict the plastic strain distribution around the particle under the same conditions but within a continuum framework. SGP results are compared to the DDD predictions.

* Corresponding authors.
  E-mail address: samuel.forest@mines-paristech.fr (S. Forest).

2. Simulation procedure

2.1. Geometry of the composite and DDD model

Fig. 1 depicts the unit cell of the simulation volume used in DDD. Because all of six faces of the simulation volume are considered as periodic boundaries, the unit cell corresponds to a 3D cubic arrangement of particles embedded in a single crystal matrix. The axes $X1$, $X2$ and $X3$ in the figure represent the geometrical (global) coordinate system attached to the spatial distribution of particles. A second crystal frame is attached to the crystal lattice of the matrix material. Accordingly, the axes $X1$, $X2$, $X3$ are located along the edges of the periodic cell. The volume fraction and radius of particle are fixed to 15% and 0.5 μm, respectively. Only one volume fraction and one particle size have been tested up to now. The chosen values are purely illustrative. The elastic properties of both the matrix and the particle are that of pure aluminium. It is assumed that the dislocation lines do not penetrate the particle. Several Frank-Read sources of 0.1 μm length, are randomly spread in the simulation volume. The initial dislocation density corresponding to the initial Frank-Read sources is set to $8 \times 10^{12}/m^2$. For simplicity, only a single slip system ($\boldsymbol{b} = 1/2[\bar{1}\,0\,1]$, $\boldsymbol{n} = (1\,1\,1)$ in the crystal frame) is considered, corresponding to system B4 according to Schmid–Boas notation. Cross-slip is forbidden during the calculation. The elastic properties of the matrix and of the particle are assumed to be isotropic and identical ($\mu = 27{,}000$ MPa, $v = 0.347$) so that no image forces need to be accounted for. Thus standard DDD simulation with periodic boundary conditions are used.

As shown in Fig. 2, two slip orientations have been selected for the DDD calculations. The first slip orientation is referred to as "simple". According to this relative orientation, the slip direction $\boldsymbol{b}$ and the slip plane normal direction $\boldsymbol{n}$ are parallel to the global directions $X1$ and $X2$, respectively. It can be described by the following orientation matrix.

$$\mathbf{X}_{simple} = \begin{pmatrix} X1 \\ X2 \\ X3 \end{pmatrix} = \begin{pmatrix} -\frac{1}{\sqrt{2}} & 0 & \frac{1}{\sqrt{2}} \\ \frac{1}{\sqrt{3}} & \frac{1}{\sqrt{3}} & \frac{1}{\sqrt{3}} \\ -\frac{1}{\sqrt{6}} & \frac{2}{\sqrt{6}} & -\frac{1}{\sqrt{6}} \end{pmatrix}$$

This slip orientation promotes the formation of dislocation pile-ups around particles separated from 0.5 μm as shown in Fig. 3. The simple configuration leads to edge and screw dislocation pile-ups located between two rows of aligned particles. The configuration also contains horizontal channels without any obstacle to dislocation glide. The width of this channel is also about 0.5 μm.

The second considered relative orientation between the crystal matrix lattice and the array of particles is labeled "X3rotate" as
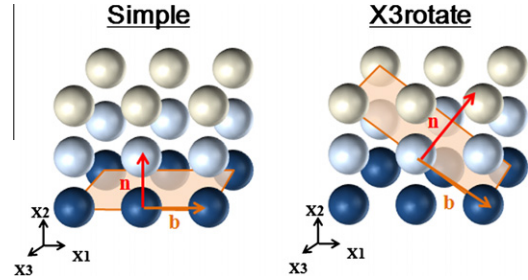

Fig. 2. Two kinds of orientation relationships between particle pattern and slip system in the matrix.
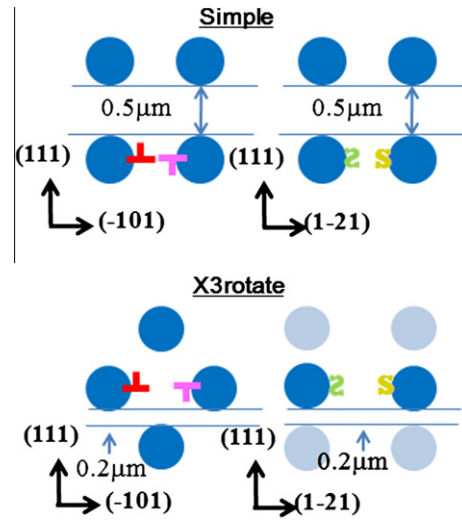

Fig. 3. 3D configuration of expected pile-up structure depending on the relative orientation of crystal matrix lattice and particle array.

shown in Fig. 2. This orientation is obtained from configuration simple by a 45° rotation with respect to $X3$ axis:

$$\mathbf{X}_{X3rotate} = \begin{pmatrix} \frac{\sqrt{2}}{2}\left(\frac{1}{\sqrt{3}} - \frac{1}{\sqrt{2}}\right) & \frac{\sqrt{2}}{2}\frac{1}{\sqrt{3}} & \frac{\sqrt{2}}{2}\left(\frac{1}{\sqrt{3}} + \frac{1}{\sqrt{2}}\right) \\ \frac{\sqrt{2}}{2}\left(\frac{1}{\sqrt{3}} + \frac{1}{\sqrt{2}}\right) & \frac{\sqrt{2}}{2}\frac{1}{\sqrt{3}} & \frac{\sqrt{2}}{2}\left(\frac{1}{\sqrt{3}} - \frac{1}{\sqrt{2}}\right) \\ -\frac{1}{\sqrt{6}} & \frac{2}{\sqrt{6}} & -\frac{1}{\sqrt{6}} \end{pmatrix}$$

Compared to simple configuration, this orientation promotes edge and screw dislocation pile-ups around more distant precipitates as shown in Fig. 3. This rotation also reduces the thickness
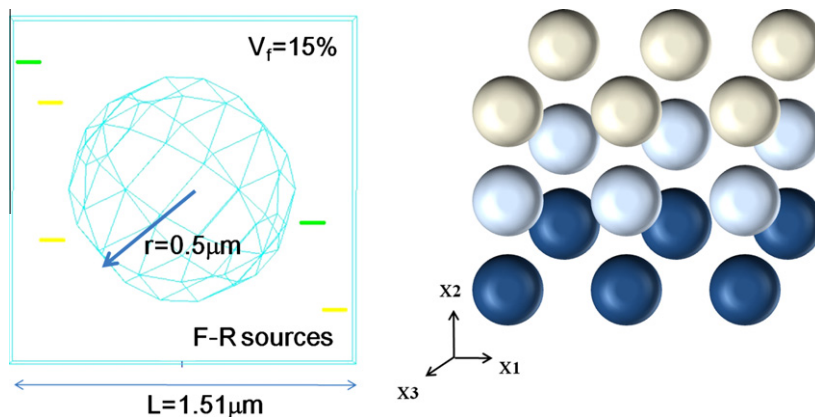

Fig. 1. DDD simulation volume (left) and three-dimensional particle arrangement (right).

of obstacle-free channels down to 0.2 µm. Each composite is subjected to homogeneous pure shear loading in slip system $[\bar{1}01](111)$.

Note that the presence of obstacle-free channels will reduce the particle induced hardening since the dislocations in the channel can propagate without any particle interaction. In this situation, the two-dimensional DDD simulations of Bassani et al. [9] have shown that the mechanical response is ideally plastic (slightly softening) with no significant channel size dependency. According to these authors, both selected orientations should lead to weak or no precipitate hardening.

However, it is worthwhile to analyze the effect of the particle induced dislocation patterns (see Fig. 3) on the mechanical response. Indeed, the full 3D interactions between mobile dislocations can lead to the formation of more complex GND distributions than expected from the simplified 2D analysis. In addition, 2D simulations only focus on pure edge infinite dislocation segments whereas 3D simulations account for curved dislocation lines (including the screw parts) and also for line tension effects.

For each DDD simulation, the dislocation distribution is analyzed by plotting the dislocation microstructure in two particular slices. A plane of normal $(1\bar{2}1)$ is selected in order to visualize the edge parts of the dislocation microstructure and a complementary plane of normal $(\bar{1}01)$ will point out the screw parts of the structure. Both slice planes contain the particle center.

2.2. Presentation of SGP model and FE simulation

The strain gradient plasticity model considered in this work has been presented in details in [8]. It is an extension of micropolar single crystal plasticity, see [10], which represents a computationally efficient approach to strain gradient plasticity. As in classical continuum plasticity, the gradient of velocity field is decomposed into elastic and plastic part:

$$H_{ij} = \dot{u}_{i,j} = H_{ij}^e + H_{ij}^p, \quad \text{with} \quad \dot{H}_{ij}^p = \dot{\gamma} n_i b_j \tag{1}$$

The stress tensor is computed from the symmetric part of $\boldsymbol{H}^e$ by means of Hooke's law. The slip γ follows from the flow rule:

$$\dot{\gamma} = \text{Max}\left(0, \left(\frac{f}{K}\right)^m\right) \text{sign } \tau \quad \text{with} \quad f = |\tau| - \tau_c \tag{2}$$

where f is Schmid's criterion function and τ, τ_c are the resolved shear stress and the critical resolved shear stress. The proposed *microcurl* model introduces a plastic microdeformation tensor χ_{ij}^p as nine additional degrees of freedom. The curl of the plastic microdeformation field is computed:

$$\Gamma_{ij} = (\text{curl}\boldsymbol{\chi}^p)_{ij} = \epsilon_{jkl}\chi_{ik,l}^p \tag{3}$$

where ϵ_{ijk} is the permutation tensor. The power of internal forces is extended to include higher order stress tensors, s_{ij} and M_{ij} that work with the plastic microdeformation and its gradient, following [11]:

$$p^{(i)} = \sigma_{ij}\dot{u}_{i,j} + s_{ij}\dot{\chi}_{ij}^p + M_{ij}\dot{\Gamma}_{ij} \tag{4}$$

The reader is referred to [8] for the derivation of the balance equations that must be fulfilled by these stress tensors. Simple linear relationships are adopted for the higher order stresses:

$$s_{ij} = H_\chi(\chi_{ij}^p - H_{ij}^p), \quad M_{ij} = A\Gamma_{ij} \tag{5}$$

where H_χ and A are the two additional parameters compared to classical plasticity. It has been shown in [8] that high values of H_χ parameters ensure that the plastic microdeformation and the plastic deformation are almost equal. As a result, Γ_{ij} is nothing but the dislocation density tensor, as defined in [4]. The physical dimension of parameter A is MPa mm². It is shown in [8] that these simple consti-
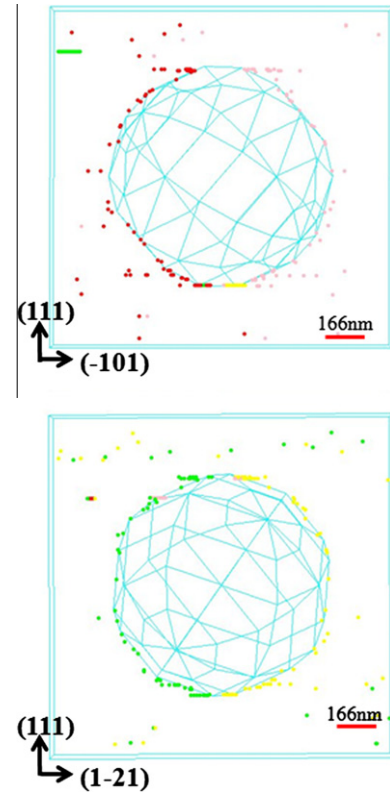

Fig. 4. Edge (top) and screw (bottom) dislocation structures around particle for the *simple* configuration, array obtained from discrete dislocation dynamics. The pictures are slices of the box but the particle is still represented in 3D.

tutive equations lead to the existence of a size dependent linear kinematic hardening component, which corresponds to the main extra-hardening effect predicted by the model for small size crystals.

The model was implemented in the finite element program Zset[1] by endowing each node of the mesh with 12 degrees of freedom corresponding to displacement vector and plastic microdeformation tensor. Implicit solver was used to solve the equilibrium equations and a fourth-order Runge–Kutta method with adaptive time-stepping was used to integrate the constitutive equations at integration points. The three-dimensional finite element mesh of the inclusion embedded in the cube matrix involves 27,568 linear tetrahedral elements corresponding to 64,188 degrees of freedom. The unit cell is subjected to the same mean simple shear loading as in the DDD simulations. Periodicity conditions of displacement and plastic microdeformations are enforced at the boundaries of the box. The values of the parameters in the *microcurl* simulations are: H_χ = 400,000 MPa and A = 0.3 MPa mm². These values induce an intrinsic length $l_s = \sqrt{A/H} = 0.9$ µm. The intrinsic length settles the range of microstructure sizes for which size effects are expected. This value is only a test value and no identification from the DDD results was attempted for this short communication. The remaining parameters are

$$\tau_c = 60 \text{ MPa}, \quad K = 1 \text{ MPa s}^{1/m}, \quad m = 10 \tag{6}$$

The viscosity parameters are such that no significant strain rate effect arises in the range of tested rates. The inclusion displays a linear elastic behavior.

The model ensures that displacement and plastic microdeformation are continuous at the interface between matrix and inclusion. The corresponding stress vector and couple stress vector are also continuous. These interface conditions have been shown in

---

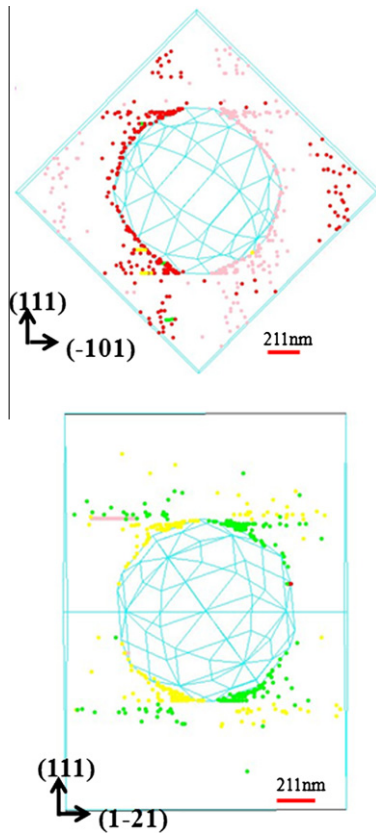[1] See http://www.nwnumerics.com, http://www.mat.ensmp.fr.

Fig. 5. Edge (top) and screw (bottom) dislocation structures around particle for the *X3rotate* particle arrays obtained from discrete dislocation dynamics.
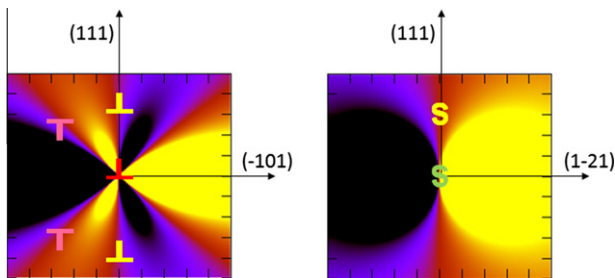

Fig. 6. Schematic stress distribution due to edge (left) and screw (right) dislocations and stable positions of incoming dislocations.

[8] to be essential for a realistic prediction of the development of GND close to interfaces. In particular, this simple constitutive framework is able to mimic the building of dislocation pile-ups.

3. Results and discussion

3.1. Dislocation structures from DDD

DDD results obtained in the case of the *simple* configuration are given in Fig. 4. The red and pink points represent positive and negative edge dislocation segments whereas yellow[2] and green points represent positive and negative screw dislocations, respectively. All results are given after 0.5% average applied shear strain ε_{12}. For this special slip orientation, only a few pile-ups are observed around the particles. The precipitate free horizontal channel concentrate the

---

[2] For interpretation of color in Figs. 1–10, the reader is referred to the web version of this article.
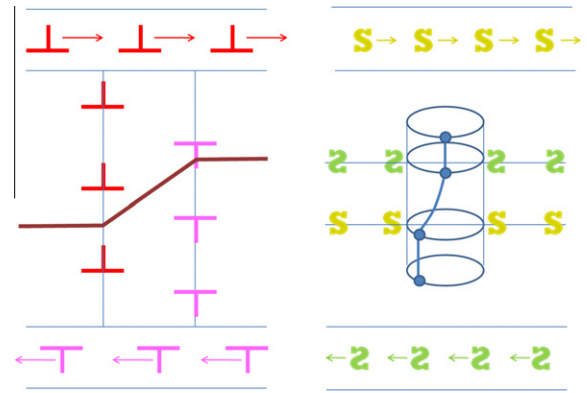

Fig. 7. Schematic diagram of edge (left) and screw (right) bands. On the left side, the horizontal bands are slip bands whereas the vertical band limited by edge walls is a kink band.
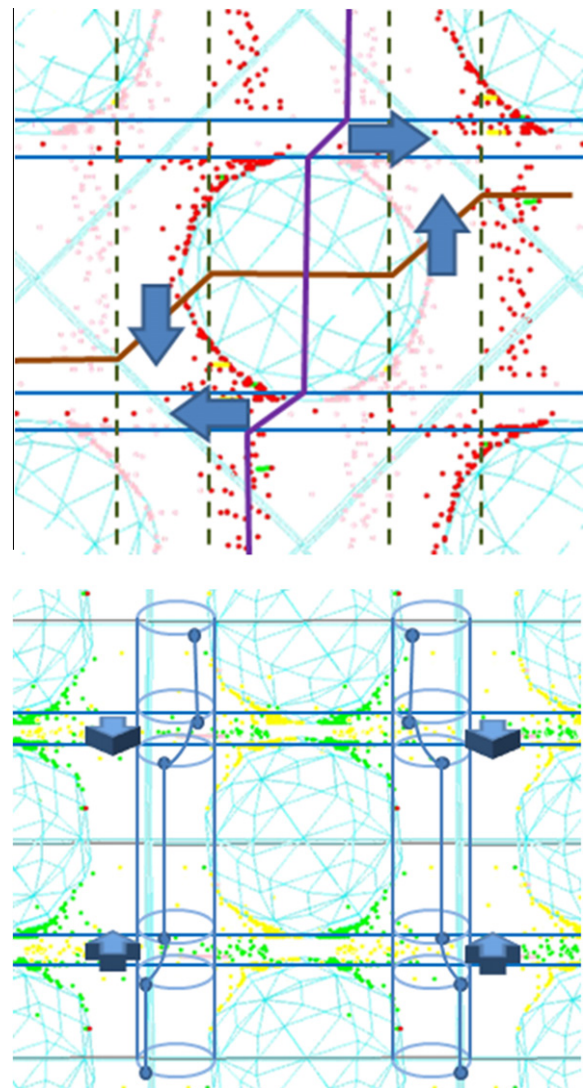

Fig. 8. Edge (top) and screw (bottom) distributions and related slip and kink bands for the *X3rotate* configuration.

dislocation activity, i.e. the plastic slip. Only a few highly mobile dislocations are observed in this channel. These results are similar to the two-dimensional calculations of [9].
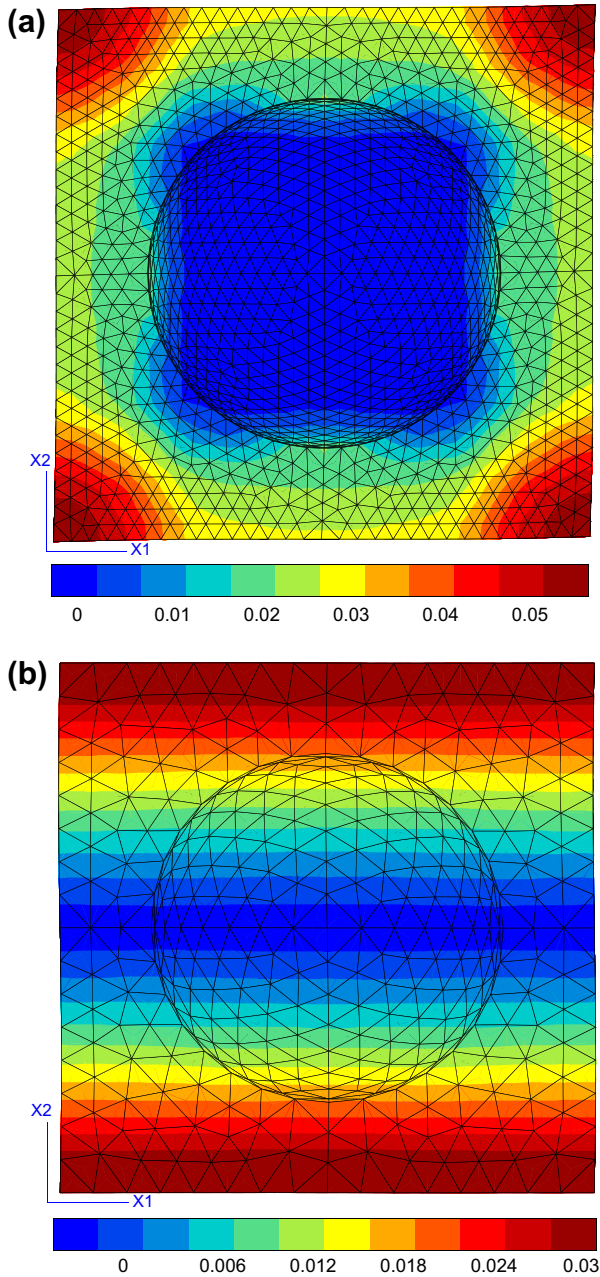
(a)

(b)

Fig. 9. Slip distribution in a slice cutting the middle of the inclusion and perpendicular to X_3: (a) classical crystal plasticity, (b) *microcurl* model. The orientation of X_1, X_2, X_3 axes correspond to the *simple* orientation. The inclusion is removed from the field so that the slip distribution around the particle can also be seen.

(a)

(b)

Fig. 10. Slip distribution in a slice cutting the middle of the inclusion and perpendicular to X_3: (a) classical crystal plasticity, (b) *microcurl* model. The orientation of X_1, X_2, X_3 axes correspond to the *X3rotate* orientation.

The situation is quite different for the *X3rotate* configuration for which remarkable edge and screw distributions are observed (see Fig. 5). One can still distinguish the precipitate free channels (narrower than in the previous case) but also dislocation walls highly visible in the edge view. The two zones bounded by the opposite edge dislocations (red and pink walls) can be interpreted as kink bands, i.e. shear bands perpendicular to the slip direction. This combination of slip and kink bands leads to a strain localization microstructure accommodating the prescribed shear stress [12,13]. The dislocation microstructures associated to the edge and screw parts are strongly different (see Fig. 5). The edge dislocations build vertical corridors and no remarkable distribution is observed in the precipitate free channel whereas the screw seg-
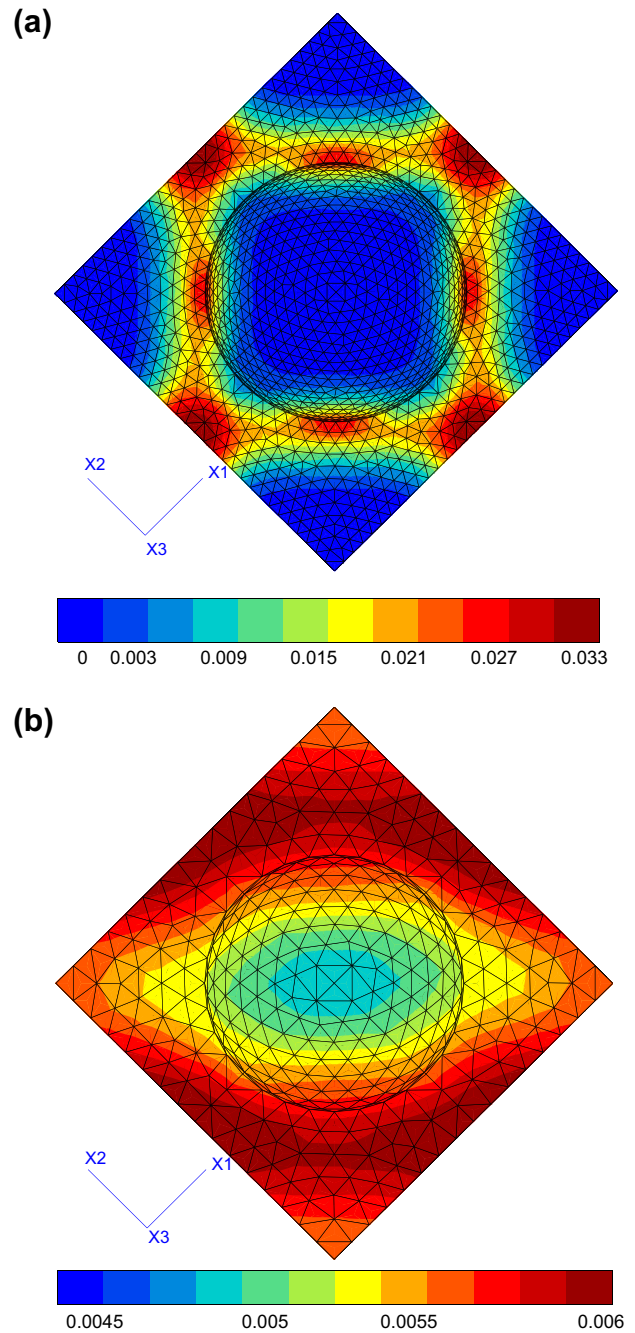
ments accumulate along the horizontal direction both above and below the particle. Edge and screw dislocations produce two kinds of shear bands as shown in Fig. 7 schematically.

The formation of such dislocation microstructures is related to the dislocation interactions. Fig. 6 qualitatively depicts the local stress field induced by infinite edge and screw dislocations. The objective is to check the stress equilibrium positions for incoming mobile dislocations. For instance, an edge dislocation with the same sign as the original dislocation (red one) is stable when located above and below (yellow symbols). Conversely, an opposite sign edge dislocation will stop on the diagonal (pink symbol). This stress interaction promotes the formation of vertical edge corridors as shown in Fig. 5. Meanwhile two screw dislocation segments can

arrange as indicated in the right part of Fig. 6. Only an opposite sign dislocation (yellow symbol) can stabilize just above or below the original screw segment (green symbol). Note that the long range stress induced by such dislocation pairs quickly vanishes leading to no hindrance to the glide of further incoming dislocations, thus promoting the formation of such horizontal microstructures.

The slip and kink bands observed in the case of the *X3rotate* configuration are depicted in Fig. 8. It was found that the edge dislocations align into horizontal slip bands and vertical kink bands around the particles. Meanwhile, the screws organize themselves into kink bands bounding the precipitate free channel. This implies that the shear deformation in the horizontal channel is accommodated both by the mobile edge dislocations and by gliding screw dislocations that eventually get immobilized.

Kink bands generally arise in two very different situations. They occur in grains or in single crystals at large deformation as strain localization modes which are predicted in the bifurcation analysis by [14]. Such kink bands have characteristic sizes (spacing or thickness) of 1 micron to tens of microns, as shown in [13]. But kink bands can also form at the early stage of deformation in the presence of obstacles like precipitates. Their width is then dictated by the spacing of the particles. In our work, due to the limitation of DDD simulations, the spacing between particles was taken to be

0.5 μm, which leads to the typical kink band width of 0.2 μm found in the simulations.

For both configurations, the mechanical response reveals a linear hardening. Configuration *simple* leads to a hardening modulus of 170 MPa and configuration *X3rotate* a hardening modulus of 210 MPa. The difference comes from the dislocation mobility in the precipitate free channels which is affected by the complex dislocation microstructure in the case of the *X3rotate* configuration. The same trend was found in [9].

3.2. Comparison with continuum crystal plasticity

As a reference, we consider first the results of FE simulations with classical continuum crystal plasticity, thus setting $A = 0$, $H_\chi = 0$ in the *microcurl*. No hardening is introduced. As a result of the elastic-perfectly plastic behavior with single slip, intense deformation bands develop around the inclusion as shown in the γ-maps of Figs. 9a and 10a for both considered orientations *simple* and *X3rotate*. In both cases, an array of horizontal slip bands and vertical kink bands is predicted. Slip is even more intense at the intersection of slip and kink bands. The slip bands predicted by the classical continuum crystal plasticity analysis are in agreement with the DDD results, see Figs. 4 and 5. However, according to these finite element analyses, the intensity of slip and kink bands
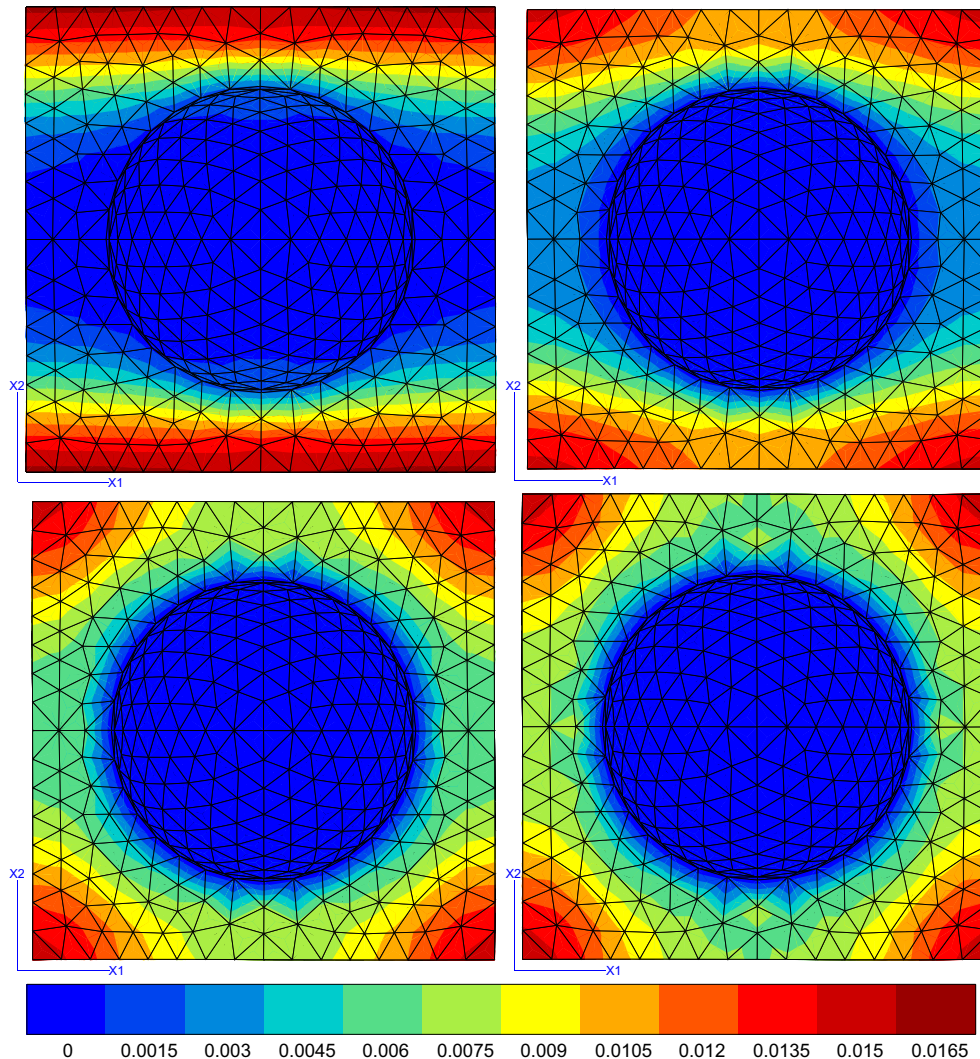

0	0.0015	0.003	0.0045	0.006	0.0075	0.009	0.0105	0.012	0.0135	0.015	0.0165	

Fig. 11. Plastic slip field in the matrix according to the microcurl model for an overall mean shear loading $H_{12} = 0.005$ of the composite unit cell for different values of A parameter in the matrix $A = 3 \times 10^{-2}$ MPa mm² and $A = 3 \times 10^{-3}$ MPa mm² (top), $A = 3 \times 10^{-4}$ MPa mm² and $A = 3 \times 10^{-6}$ MPa mm² (bottom).

are identical. This is not the case in DDD simulations for which the kink bands for the orientation *simple* are of very limited intensity, see Fig. 4. In DDD simulations, slip and kink bands behave differently because kink bands are associated with dislocation wall formations. This is not correctly described by the classical plasticity analysis.

In contrast, simulations based on the *microcurl* model with $A = 0.3$ MPa mm^2 show a different behavior of slip and kink bands, as shown in Figs. 9b and 10b. This is due to the fact that slip in vertical kink bands induces non-homogeneous lattice rotation and therefore non-vanishing dislocation density tensor. According to Eq. (5), the higher order stress increases in kink bands, which was shown in [8] to induce linear hardening. As a result of locally increasing stress levels inside kink bands close to the inclusion, slip remains limited whereas unlimited slip can take place in the horizontal slip bands. That is why the vertical bands almost disappeared in Fig. 9b to the benefit of horizontal slip bands, in agreement with DDD results. For the *X3rotate* orientation, slip inside the vertical channels is also smaller than the amount of slip in the horizontal channels. The fact that kink bands remain active for this orientation is in agreement with the DDD results.

The maps of plastic slip γ for classical and *microcurl* simulations are given for $H_{12} = 0.01$ applied average glide. It can be noted that the slip distribution is much more localized for classical plasticity than for *microcurl* simulations. This is due to the hardening induced by strain gradients in the latter case. If parameter A is decreased, keeping the same inclusion size, the intensity of the kink band increases continuously. When A is vanishingly small, the pattern found is the same as for classical crystal plasticity, as expected. The Fig. 11 shows the progressive development of the kink bands for A in the matrix ranging from 0.03 MPa mm^2 to $A = 3 \times 10^{-6}$ MPa mm^2, keeping the value of $A = 0.3 \times 10^{-7}$ MPa mm^2 in the inclusion, as recommended in [8].

Good qualitative agreement is found for the prediction of deformation structures in the composite for DDD and SGP models. However a quantitative comparison on dislocation density tensor values close to interfaces between matrix and inclusion is postponed to future work, because finer finite element meshes will be required for this local analysis.

4. Conclusion

The dislocation microstructures formed around particles have been investigated in the case of a periodic arrangements of particles for two slip system orientations using two numerical tools: three-dimensional DDD and SGP model. In DDD simulations, remarkable slip and kink band structures around the particles have been found. It is shown that kink bands, associated with high GND densities enhance the hardening rate. The GND content close to

particles is essentially linked to the formation of kink bands in addition to slip bands in a characteristic finite zone which depends on slip system orientation with respect to particle spatial distribution.

Description of such detailed kink-slip band structures does not seem to exist in literature for metal matrix composites. In [15], dislocation structures are shown but not examined in detail. Observation of kink bands would require systematic EBSD measurements around particles which are still not available with the necessary resolution. Also, the structures predicted by our simulations are simplistic in the sense that we did not account for multislip and cross-slip. That is why the comparison with experimental evidence remains very limited.

Future work will be successively devoted to the consideration of cross-slip effects, introduction of multi-slip and, finally, determination of particle size effect on plastic flow and cyclic hardening. A proper identification of the value of parameter A will require comparison of the hardening curves of the composite for various inclusion sizes.

References

[1] F.J. Humphreys, Acta Metallurgica 27 (1979) 1801–1814.
[2] M. Calcagnotto, D. Ponge, E. Demir, D. Raabe, Materials Science Engineering A 527 (2010) 2738–2746.
[3] V. Taupin, S. Berbenni, C. Fressengeas, O. Bouaziz, Acta Materialia 58 (2010) 5532–5544.
[4] P. Cermelli, M. Gurtin, Journal of the Mechanics and Physics of Solids 49 (2001) 1539–1568.
[5] S. Forest, R. Sedláček, Philosophical Magazine A 83 (2003) 245–276.
[6] C.S. Shin, M.C. Fivel, M. Verdier, K.H. Oh, Philosophical Magazine 83 (2003) 3691–3704.
[7] M. Verdier, M. Fivel, I. Groma, Modelling and Simulation in Materials Science and Engineering 6 (1998) 755–770.
[8] N. Cordero, A. Gaubert, S. Forest, E. Busso, F. Gallerneau, S. Kruch, Journal of the Mechanics and Physics of Solids 58 (2010) 1963–1994.
[9] J. Bassani, A. Needleman, E. Van der Giessen, International Journal of Solids Structures 38 (2001) 833–853.
[10] J. Mayeur, D. McDowell, D. Bammann, Journal of the Mechanics and Physics of Solids 59 (2011) 398–422.
[11] M.E. Gurtin, Journal of the Mechanics and Physics of Solids 50 (2002) 5–32.
[12] S. Forest, Modeling slip, Acta Materialia 46 (9) (1998) 3265–3281.
[13] D. Kuhlmann-Wilsdorf, Acta Materialia 47 (1999) 1697–1712.
[14] R. Sedláček, W. Blum, J. Kratochvil, S. Forest, Metallurgical and Materials Transactions 33A (2002) 319–327.
[15] T. Gustafson, P. Panda, G. Song, R. Raj, Acta Materialia 45 (1997) 1633–1643.